Irradiation of plutonium tributyl phosphate complexes by ionizing alpha particles: a computational study

Damien Tolu, Dominique Guillaumont, Aurélien de la Lande

▶ **To cite this version:**

Damien Tolu, Dominique Guillaumont, Aurélien de la Lande. Irradiation of plutonium tributyl phosphate complexes by ionizing alpha particles: a computational study. Journal of Physical Chemistry A, 2023, 127 (34), pp.7045. 10.1021/acs.jpca.3c02117 . cea-04662956

HAL Id: cea-04662956

https://cea.hal.science/cea-04662956v1

Submitted on 26 Jul 2024

HAL is a multi-disciplinary open access archive for the deposit and dissemination of scientific research documents, whether they are published or not. The documents may come from teaching and research institutions in France or abroad, or from public or private research centers.

L'archive ouverte pluridisciplinaire **HAL**, est destinée au dépôt et à la diffusion de documents scientifiques de niveau recherche, publiés ou non, émanant des établissements d'enseignement et de recherche français ou étrangers, des laboratoires publics ou privés.

Irradiation of plutonium Tributyl Phosphate complexes by ionizing alpha particles: a computational study

Damien Tolu,[*,†,‡] Dominique Guillaumont,[†] and Aurélien de la Lande[*,‡]

†*CEA, DES, ISEC, DMRC, Université Montpellier, Marcoule, 30207 Bagnols sur Cèze, France*

‡*Institut de Chimie Physique, CNRS, Université Paris Saclay, 15 Avenue Jean Perrin, 91405, France*

E-mail: damien.tolu@cea.fr; aurelien.de-la-lande@universite-paris-saclay.fr

Abstract

The PUREX solvent extraction process is widely used for recovering uranium and plutonium from spent nuclear fuel, it uses an organic solvent made up of TriButyl Phosphate (TBP). The emission of ionizing particles such as alpha particles, resulting from the decay of plutonium, make the organic solvent vulnerable to degradation. Here, we study the ultra-short time alpha irradiation of tributylphosphate (TBP) and $Pu(NO_3)_4(TBP)_2$ complex formed in the PUREX process. Electron dynamics is propagated by Real-Time Time-Dependent Auxiliary Density Functional Theory (RT-TD-ADFT). We investigate the use of previously proposed Complex Absorbing Potentiel (CAP) in energy space to treat secondary electron emission. Basis set and exchange correlation functionals effects with CAP are reported as well as a detailed analysis of the CAP parametrisation. Preliminary results on water molecule and then on TBP show that the phenomenological nature of the CAP parameters induces an adapted

choice of their values for each studied system. Irradiation of free and complexed TBP shows an influence of the ligands in the variation of atomic charges at the femtosecond time scale. An accumulation of atomic charges in the alkyl chains of TBP is observed in the case where the nitrate groups are predominantly irradiated.

Introduction

The effect of ionising radiations on matter has been known and studied since the late 19th century[1,2]. Their range of action extends from the extreme conditions of interstellar space to nuclear power plant reactors[3,4]. Ionizing radiations are also central players is nuclear medicine, and notably radio-therapies[5,6] as well as in food industry for sterilization purposes[7]. In the nuclear fuel cycle, one issue is to achieve the extraction of radioactive elements (actinides) during the recycling of nuclear fuel using organic extractant molecules, which are susceptible to degradation due to ionizing radiations. Research groups are therefore pursuing a strategy to design radio-resistant extracting molecules. In this perspective, understanding the degradation mechanisms of extractant molecules is mandatory.

Experimental methods such as gas chromatography or mass spectrometry permit the identification of degradation products resulting from the passage of ionising radiation in matter[8–10]. Pulsed irradiation experiments have made it possible to trace the chronology of these mechanisms, both intra- and inter-molecular, down to the picosecond scale[11,12] in real-time. There is also work studying indirect irradiation by secondary electrons emitted with the medium[13]. Finally, the development of pump-probe spectroscopy at ultrashort times now makes it possible to probe matter on the attosecond scale[14], and to understand electronic rearrangements in the case of irradiation with ionising electromagnetic waves[15].

However, many grey areas remain out of reach of experimental techniques especially when that are considering ultrafast (<ps) responses. Numerical simulations are therefore essential to unravel the origin of these phenomena and to link them to experimental data. This is particularly true for systems such as nanoparticles[16], charge transfer mechanisms or elec-

tronic rearrangements[17], biological systems[18], or irradiation by massive ionising particles. Among theoretical chemistry approaches, time-dependent DFT (TD-DFT), introduced by Runge and Gross is one of the most appealing[19]. It constitutes the basis of the first numerical propagations developed with the time-dependent local density approximation (TD-LDA) method in the 90's[20–22]. These propagations first used a linear response formalism, suitable for small perturbations[23], but were very quickly improved by explicitly propagating the electron density over time[21]. The so-called real-time (RT-) TD-DFT method gives access to non-adiabatic phenomena and strong perturbations. Recently we have extended RT-TD-DFT to the Auxiliary DFT (ADFT) framework opening up the possibility to deal routinely with large molecular systems[24]. In ADFT, auxiliary gaussian functions are combined with basis functions to decrease the total number of terms in the repulsive Coulomb and exchange-correlation parts. The fitted electron density is obtained by minimization of self-interaction error as illustrated in[25]. Electron dynamics calculations have been used to study ultrafast processes such as proton transfers as in the work of Sharma and Fernández-Serra[26], the ionisation and degradation of biological molecules subjected to a beam of ionising particles[18,27,28], or 2D chemical systems[29]. RT-TD-DFT has also found promising applications to the calculation of electronic stopping power of fast ions in matter[30–34]. We finally note the work of Dinh et al to calculate the resonance energy of a secondary electron bound state capture[35].

We are interested in the irradiation of tributyl phosphate (TBP) by alpha particles, an extractant molecule mainly used in the PUREX (Plutonium, Uranium, Reduction, Extraction) process for recycling uranium (VI) and plutonium (IV). Our objective is to unravel the mechanisms of energy deposition upon irradiation and the ultrafast responses triggered by irradiation of the TBP ligand or heavy elements chelated by TBP. This knowledge would bring valuable information to understand the early mechanisms leading to a loss of extracting proprties of TBP solutions. To this end, we aim here at simulating the interaction of the fast ions with the electron cloud of TBP and Pu complexes.

Upon alpha decay of a plutonium nucleus (equation 1) most of the energy released is transferred to the momentum of the alpha particle (Eq. 1). As a consequence of the mass difference between the uranium and helium nuclei, the energy released amounts to a few MeV.

$$^{239}Pu \longrightarrow ^{235}U + ^{4}He \tag{1}$$

For this range of kinetic energy, an emitted alpha particle rapidly travels away from the heavy nucleus and strongly interacts with the surrounding molecules. For the electrons of the irradiated molecules, the passage of the projectile implies a strong perturbation of the external potential leading to electronic transitions (*i.e.* excitations). A 5 MeV alpha particle travels at a speed of 0.16 Å/as and would get through a small organic molecule in a few tens of attoseconds, say 50 as. Because of the time-energy uncertainty principle ($\Delta E.\Delta t \geq \hbar/2$), such a transient collision would be associated with an energy uncertainty of at least 6.5 eV. Collision would thus result in the formation of a superposition of a large number of quantum states. This cannot be described by linear response methods[36], but for example by RT-TD-DFT. Despite possible shortcomings of RT-TD-DFT to described matter under strong field irradiation[30,37,38], which are related to approximation in exchange correlation functional approximations, RT-TD-DFT out-performs time-dependent wave function methods, enabling the study of larger systems.

A major difficulty encountered when simulating ionizations is the description of so-called secondary electrons in non-bonding states. A common procedure to address this issue is to add complex absorbing potentials (CAP) to avoid non-physical effects of auto-ionizations and the reflection of the electron density at the edges of simulation grids. CAPs were introduced in the 90's[39] to deal with diffuse reactions such as collisions between atoms[40,41]. It was introduced as an alternative to mask functions[42]. By adding a complex component to the system's Hamiltonian, the electron density is gradually absorbed beyond a threshold distance[37,43–63]. CAPs have been shown to be very effective when coupled with multiconfigurational methods[64–66], coupled-cluster methods[67–75], MRCI (Multireference Configura-

tion Interaction) potential energy surfaces[76–79], Extended Tremblay and Carrington (ETC) method using GENIUSH-CAP code[80], Analytic Continuation of the Coupling Constant (ACCC) methods[81], Time Dependent Density Functional Theory (TD-DFT)[82], and Electron Attachment Algebraic-Diagrammatic Construction (EA-ADC) method[83] in the study of metastable resonance states for anionic molecular systems. Its applications are extended in the generation of high harmonic generation (HHG) spectra with RT-TD-DFT[84], TD-CIS[85] or Time-Dependent Schrodinger Equation (TD-SE) with core dynamics[86], in non-Hermitian exceptional point (EPs) degeneracies[87], or in ionisation and excitation of systems with coupled-cluster[88], or Time-Dependent Configuration Interaction (TD-CI)[89] methods. When using local (atom-centered) basis sets a drawback may become the computational cost generated by CAP. On one hand, the CAP needs to be placed sufficiently far away from the molecules so that bound electrons will not be absorbed during the simulation. For the simulation of ion-molecule collisions, we found that a minimum of 10 Å was advisable[90]. On the other hand, diffuse basis set functions are needed to cover the space between the molecules and the CAP, thereby increasing the computational cost of the simulations, sometimes drastically.

Another form of CAP was proposed by Klamroth and co-workers in their investigation of photoionization of diatomic molecules by TD-CI[91]. Electrons were absorbed based on a energy-level criterion. A similar approach was developed by Niehaus and co-workers in the context of TD-DFTB (DFT Tight Binding)[92] to simulate extreme UV (XUV) ionization of the caffeine molecule. Lopata et al. developed such an energy CAP for TD-DFT in order to simulate X-ray and XUV spectra[93,94]. Non-Hermitian real-time TD-DFT offers an efficient approach to interpret near-edge X-ray absorption spectra (XAS) spectra provided that proper attention is paid to the shift of the non-bounding energy levels .

In this article we assess the reliability of energy CAP in the context of fast ion-molecule collisions. Where the target molecule is an organic ligand (TBP) free or incorporated into a plutonium(IV)[95,96] ($Pu(NO_3)_4(TBP)_2$ as in the PUREX process[97]). After introducing the methodology, we report on a sensitivity analysis of the CAP parameters, which we think

will be of interest for other potential users of energy CAP at the TD-DFT level. We further investigate the profiles of deposited energy and the post-collision charge migrations, notably the influence of exact exchange on simulated results.

Methodology

All calculations have been carried out with a modification of DFT-based code deMon2k (version 6.1.6)[98]. The geometries of TBP and $Pu(NO_3)_4(TBP)_2$ were optimized at the Auxiliary Density Function Theory (ADFT) level of theory[99,100]. The Coulomb as well as the exchange-correlation contributions to the Kohn-Sham potential were calculated using auxiliary electron densities obtained by variational density fitting[99,100]. We first determined the ground state electron density by a Self-Consistent-Field (SCF) calculation in absence of the projectile. Then, we simulated the response of the electron cloud to alpha particle irradiation by RT-TD-ADFT. Initially, the projectile is placed at the edge of a 40 Å radius sphere centered at the centre of mass of the molecule. This distance is large enough to avoid Kohn Sham potential discontinuities which would lead to spurious perturbation during the first propagation steps. The projectile had kinetic energy of 0.5 or 5.1 MeV and is therefore accurately described as a point-charge particle.

The electron density is propagated in time using the evolution operator $U(t, t_0)$ and the numerical solution of equation 2. For this purpose, the operator $U(t, t_0)$ is developed by discretizing time into n intervals (equation 2)

$$P(t) = U(t, t_0)P(t_0)U^{\dagger}(t, t_0) \quad ; \quad U(t, t_0) = \prod_{i}^{n-1} U(t_i + \Delta t, t_i) \tag{2}$$

with $U(t_i + \Delta t, t_i) = \mathcal{T} \exp\left(-i \int_{t_i}^{t_i+\Delta t} H(t')dt'\right)$, $\mathcal{T}$ the time-ordering operator, $P(t)$, $H(t)$ the density matrix and the system's Hamiltonian at instant t, $U(t, t_0)$ the evolution operator, and Δt the propagation time step.

The integration of the Hamiltonian over time in $U(t_i + \Delta t, t_i)$ is approximated by the

second-order Magnus propagator (equation 3).

$$-i \int_{t_i}^{t_i+\Delta t} H(t')dt' \approx -iH'\left(t + \frac{\Delta t}{2}\right)\Delta t \tag{3}$$

The computation of the propagator (matrix exponentiation) is evaluated by a Taylor series of order 60. During the propagation, the projectile follows a linear, uniform motion and its interaction with the molecular system is represented by an electrostatic potential that follows a Coulomb law (equation 4).

$$E^{proj} = -\int \rho(\boldsymbol{r}, t)\phi_{proj}(\boldsymbol{r}, t)d\boldsymbol{r} + \sum_A Z_A \boldsymbol{R}_A \phi_{proj}(\boldsymbol{r}, t) \tag{4}$$

Where ρ is the electron density, ϕ_{proj} is the potential generated by the projectile, $\boldsymbol{r}$ is the electron position, Z_A and $\boldsymbol{R}_A$ are the atomic charge and coordinate vector of nucleus A, respectively.

The deposited energies are negligible compared to the initial energy of the projectile. Therefore we assume that its velocity vector remains constant throughout the simulations. Only the coordinates are updated at each time step. Furthermore, due to their realtive masses, the electrons and nuclei of the system move with different propagation times. In the attosecond timescale, only the motion of the electrons is appreciable, while the nuclei are frozen in virtue of the Born-Oppenheimer approximation.

The CAP is calculated at the beginning of the RT-TD-ADFT simulation as $CAP = C(t)\Lambda C^{\dagger}(t)$ in the MO basis, where C is the ground state MO coefficients matrix. The Λ matrix is a diagonal matrix (equation 5)

$$\Lambda = \begin{pmatrix} \gamma_1 & 0 & \dots & 0 \\ 0 & \gamma_2 & \dots & 0 \\ \vdots & \vdots & \ddots & \vdots \\ 0 & 0 & \dots & \gamma_M \end{pmatrix} \tag{5}$$

The matrix terms γ_i are computed by 6

$$\gamma_i = \begin{cases} 0 & \tilde{\varepsilon} \leq 0 \\ \gamma_0[\exp(\xi\tilde{\varepsilon} - 1] & \tilde{\varepsilon} > 0 \end{cases} \tag{6}$$

with γ_0 and ξ being parameters controlling the absorption of electrons in the i state, and $\tilde{\varepsilon}_i = \varepsilon_i - \varepsilon_0$ the i MO shifted energy by the ε_0 term. Indeed, within the Kohn-Sham DFT framework with the exact exchange-correlation functional, $EA = -E_{LUMO}$ with E_{LUMO} being the Lowest Unoccupied Molecular Orbital (LUMO) energy. This is actually not true in practice for most functionals[101–103]. ε_0 is thus introduced to shift the underestimated energies of the Kohn-Sham orbitals of unbound electrons. This is done by forcing the EA to be equal to minus the shifted LUMO energy. The electron affinity (EA) is calculated as follows from two independent SCF calculations:

$$EA = E_N - E_{N+1} \tag{7}$$

where E_N is the total energy of the system, E_{N+1} the total energy of the anion. In Lopata et al.[93,94], ε_0 was obtained after electron affinity interpolation for the virtual orbitals of the system. To avoid this practical solution requiring perturbative TD-DFT calculation of the anion, we started from the equation 8

$$(E_{LUMO} + \varepsilon_0) = -EA \Leftrightarrow \varepsilon_0 = (-1)(E_{LUMO} + EA) \tag{8}$$

in order to estimate ε_0. We note that as a result of the ionization process, the electron

affinity changes and so does the term ε_0. Therefore, the CAP should in principle be recomputed on-the-fly. In practice though, we did not consider this possibility here and computed the CAP once for all at the beginning of the simulations. We will devote a section to the tuning of CAP parameters in the Results section. The MOs lifetimes are calculated according to equation 9

$$\tau_i = \frac{1}{2\gamma_i} \tag{9}$$

A correct description of the ejected electrons goes through a good description of unoccupied states and requires the use of extended basis sets. The work of Bruneval and co-workers shows that the use of different size of basis sets is a reasonable choice. The closer the atoms are from the point of impact, the larger the number of basis functions should be. However, this method requires a customized set of basis functions for each trajectory and makes the analysis of the properties more difficult. Furthemore, for plutonium complexes, the use of large basis sets tends to cause convergence problems during the SCF procedure.

To avoid this issue, a unique basis set was built for light atoms using cc-PVTZ. For plutonium(IV), a quasi relativistic effective core potential (ECP) replacing 82 inner shell core electrons including 5f electrons is used with the related basis set for valence electrons[104].

The VWN[105], PBE[106], LCPBE[107] and PBE0[108] functionals are used to calculate the exchange-correlation energy and the auxiliary density is determined using the GEN-A2* auxiliary functions. During unperturbed electron propagation, the SCF convergence criterion must be fine enough to verify the stability of the energy and electron number. For this purpose, it is recommended to initialise the convergence threshold values for energy and axiliary density error of 10^{-9} and 10^{-7} Ha respectively[109].

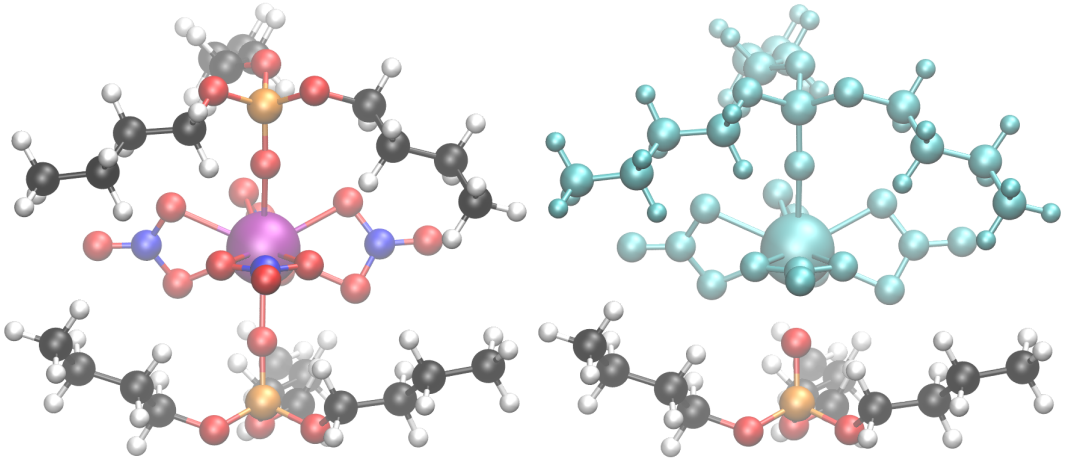

(1) (2)

Figure 1: Studied systems : (1) $Pu(NO_3)_4(TBP)_2$ (2) TBP with ghost atoms (purple) to preserve a unique basis set

The simulation box is created starting with the complex $Pu(TBP)_2(NO_3)_4$ geometry. For the calculation of free-TBP without plutonium, ghost atoms are placed for all the others atoms (figure 1) in order to retain the same basis set than in $Pu(TBP)_2(NO_3)_4$.

Results and Discussion

Electronic propagation parameters

This section is devoted to the determination of the main CAP parameters, namely ε_0, γ_0 and ξ, during the irradiation by an alpha particle.

We start by evaluating the influence of the propagation time step on the deposited energy, the amount of ionisation and the charge flow after alpha particles irradiation. To this end, we consider a simple molecule, i.e. H_2O. The CAP parametrization protocol is then transposed to the TBP molecule and to the $Pu(NO_3)_4(TBP)_2$ complex. We achieve the density matrix propagation via an iterative second order Magnus propagator. The total duration of all simulations is 15 fs. A suitable propagation time step (t_e) is estimated by the velocity of the projectile, but must also be consistent with the velocity of the phenomenon under study. For

a 5.1 MeV alpha particle, the distance travelled is estimated to be 0.1 Å in 1 as whereas it is 0.05 Å for a 0.5 MeV alpha particle. The time step must be small enough to minimize the propagation error in the equation 4, and to estimate the maximum energy deposited in the system after the addition of an absorbing complex, while keeping the cost of the calculations acceptable. The simulations are carried out with the PBE functional, the atomic basis set cc-PVTZ and the auxiliary basis set GEN-A2*. A CAP is used with $\gamma_0 = 0.1$ Ha/$\xi = 0.05$ Ha^{-1} and $\gamma_0 = 0.025$ Ha/$\xi = 0.05$ Ha^{-1} for 5.1 and 0.5 MeV alpha particles, respectively. In Table 1, the deposited energy E_d, the number of emitted electrons El_{abs} and the root mean square deviation (RMSD) of the atomic charges are collected for different values of t_e (namely 0.05, 0.1, 0.5 and 1 as). The RMSD values of the atomic charges are calculated relative to the values obtained for $t_e = 0.05$ as. The amount of deposited energy (E_d) depends on the propagation time step. For a 5.1 MeV alpha particle E_d increases from 2,263 to 2,424 kcal.mol^{-1} between 1 as and 0.5 as,and is then increases again to 2,463 kcal.mol^{-1}. As this high energy, the time step of 1 as is not short enough to fully resolve the irradiation process. As expected E_d is less sensitive to the chosen time step for a 0.5 MeV alpha particle. For both kinetic energies, the amount of emitted electron and the charge fluctuations are weakly sensitive to the value chosen for t_e.

Table 1: Properties calculated from electronic propagations. t_e the propagation time step (as), E_α the initial kinetic energy of the projectile (MeV), E_d the deposit energy (kcal.mol^{-1}) , El_{abs} the number of electrons absorbed, and RMSD the root mean square deviation of the atomic charge of atom X.

	$E_\alpha = 5.1$ MeV					$E_\alpha = 0.5$ MeV				
			RMSD					RMSD		
t_e	E_d	El_{abs}	O	$H_{(1)}$	$H_{(2)}$	E_d	El_{abs}	O	$H_{(1)}$	$H_{(2)}$
1 as	2,263	0.68	0.024	0.013	0.013	6,453	2.62	0.017	0.012	0.011
0.5 as	2,424	0.70	0.001	0.001	0.001	6,480	2.62	0.001	0.001	0.001
0.1 as	2,462	0.70	0.000	0.000	0.000	6,489	2.62	0.000	0.000	0.000
0.05 as	2,463	0.70	0.0	0.0	0.0	6,490	2.62	0.0	0.0	0.0

Complex Absorbing Potential

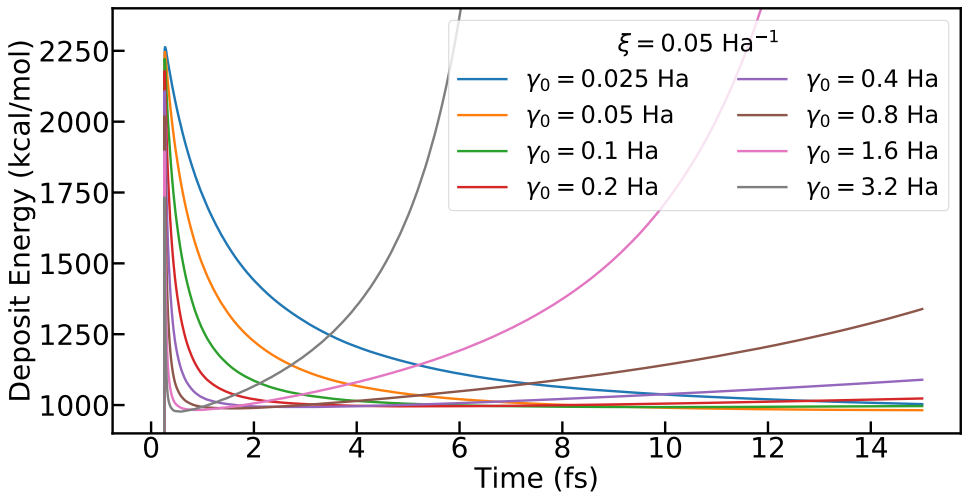

(1)

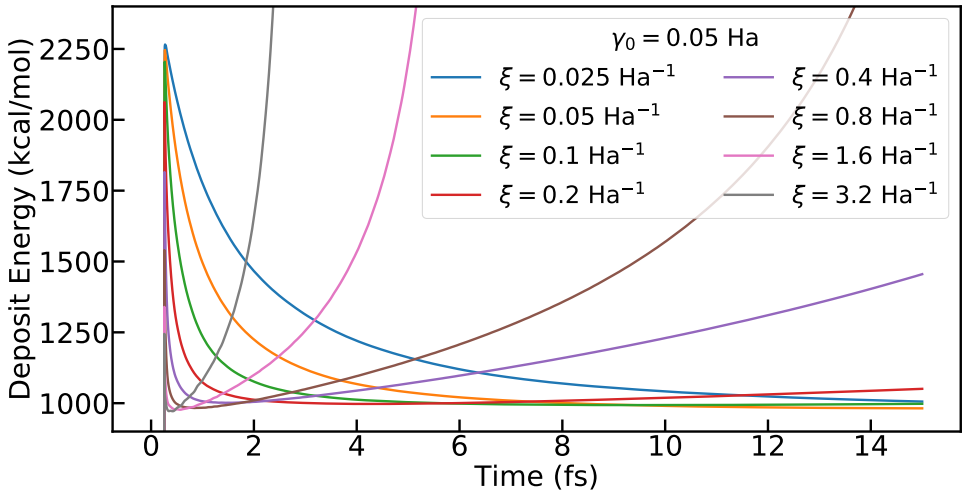

(2)

Figure 2: Deposition energy profiles with the PBE functional. Upper panel (1): variation of γ_0, keeping ξ at 0.05 Ha^{-1}. Lower panel (2) variation of ξ, keeping γ_0 at 0.05 Ha

The parameters γ_0 and ξ contribute to define the lifetime of excited electrons in high energy MO (equations 6 and 9). Here, we investigate the influence of these parameters on the energy deposition profiles, while still considering the irradiation of a water molecule. The PBE functional is used, setting ε_0 to 0.098 Ha via Eq. (8) together with the cc-PVTZ and GEN-A2* orbital and auxiliary basis sets. The results are collected in figure 2, where the plot

$\Delta E(t_i) = E(t_i) - E_{ref}$ is shown, with $E(t_i)$ the total energy at time t_i and E_{ref} the ground state energy obtained through a self-consistent-field procedure. We expect a sharp increase in the deposit energy at the moment of the collision (around 0.25 fs after the beginning of the simulations), followed by a decrease in energy, which would be a consequence of the absorption of electrons by the CAP. After complete absorption of the emitted electrons, the energy stabilizes to a steady value. Electrons present in orbitals whose lifetime is longer than the duration of the simulation do not have the time to be absorbed and contribute very little to the decrease in energy. Such typical profiles are obtained for most CAP parameters, but not for γ_0 higher than 0.1 Ha or for ξ higher than 0.1 Ha^{-1}. In the latter cases, a divergence of the total energy is observed after the energy drop. This evolution indicates unphysical dynamics reflecting massive absorption of valence and core electrons. Otherwise, when considering the stable dynamics, when we increase the values of γ_0 or of ξ, the lifetime of electrons in non-bonding orbitals decreases accelerating the post-collision energy decrease, as expected. The stability of RT-TD-DFT simulations using energy-space CAP is highly sensitive to the choice of parameters. Based on the data reported here, we recommend using γ_0 values that do not exceed 0.1 Ha.

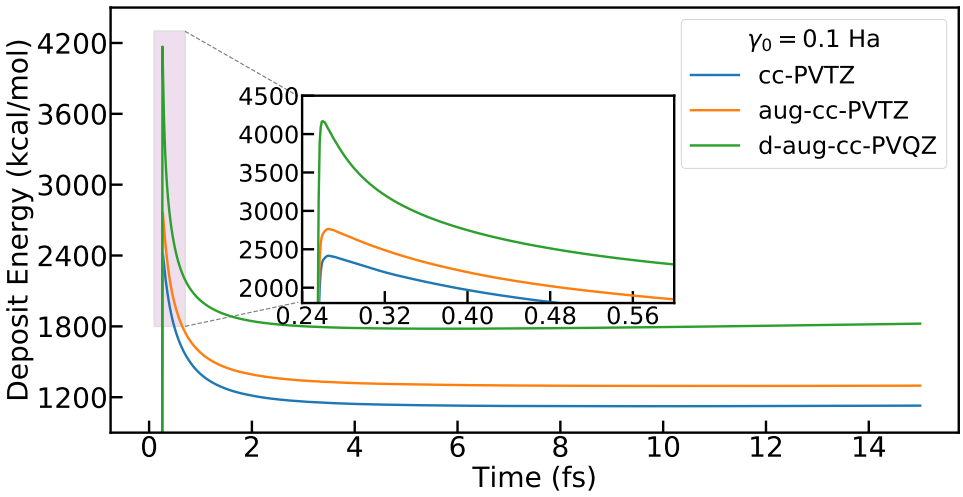

Figure 3: Deposited energy as a function of time at the RT-TD-ADFT level, with PBE functional. The blue, orange and green curves correspond to cc-PVTZ, aug-cc-PVTZ and d-aug-cc-PVQZ atomic basis sets. The value of γ_0 is assigned to 0.1 Ha while ξ is fixed at 0.05 Ha^{-1}

.

It is known that the amount of deposited energy by the projectile, or equivalently the electronic stopping power, is strongly dependent on the basis set. While some codes rely on plane-waves[110–112], deMon2k uses atom-centered Gaussian type orbitals to expand the Kohn-Sham MO. Bruneval et al., studying the electronic stopping power in solid models (eg. Li, Al), proposed to use of mixed bases, with richer basis positioned on the atoms near the projectile's propagation line and smaller bases for distant atoms. This was argued to be an effective way to describe the multiple excitations of electrons in energy levels. This is in order to limit the computational cost of the simulations[113]. Although appealing, this strategy is not applicable here because we have to deal with heterogenous molecules. The effects of an irradiation on the electron density are local, centred around the trajectory. Unitarily, it is possible to define an optimal atomic basis set for each of them. However, sampling implies a comparison of all the simulations, which can only be done by keeping the same atomic basis functions from one trajectory to another. Following the strategy used in[113] would introduce strong basis set effect.

Figure 3 shows the deposited energies in a water molecule for which the atomic basis sets

cc-PVTZ, aug-cc-PVTZ and d-aug-cc-PVTZ are used. We use an energy CAP with $\gamma_0 =$ 0.1 Ha and $\xi = 0.05$ Ha^{-1}. The parameter ε_0 was determined for each calculation, shifting the higher MO eigenvalues by 0.098, 0.046 and 0.058 Ha for cc-PVTZ, aug-cc-PVTZ and d-aug-cc-PVTZ respectively.

The richer the Gaussian basis set, the higher the deposit energy increases. For d-aug-cc-PVTZ the number of emitted electrons is higher than for the other two basis sets, but the final deposit energy is also more important. This can be explained by the quantities of binding orbitals described. Indeed, the CAP defines lifetimes for non-bonding orbitals only. Ten binding, but non-populated, orbitals are described by d-aug-cc-PVTZ, they contribute to the increase of the total energy of the system without the CAP being able to influence their lifetimes. This same number falls to two for the atomic basis functions aug-cc-PVTZ and cc-PVTZ. The difference in energy of the latter is explained by a longer occupation time of the electrons in the first non-bonding orbitals with aug-cc-PVTZ.

Table 2: Periods of time following irradiation of H_2O, for which energy stability is reached and between -5.10^{-5} and $+5.10^{-5}$ kcal.mol $^{-1}$. The simulations were performed at the RT-TD-ADFT level, the cc-PVTZ atomic base, and the GEN-A2* auxiliary base.

γ_0	0.025	0.05	0.1	0.2	0.4	0.8	1.6	3.2
PBE	$> 5.10^{-5}$	13.9−14.9 fs	6.7−13 fs	3.9−7 fs	3.1−4 fs	div.	div.	div.
LCPBE	$> 5.10^{-5}$	10.7−13.3 fs	5.4−7.3 fs	3−3.6 fs	div.	div.	div.	div.
VWN	$> 5.10^{-5}$	14.1−14.8 fs	7.3−12.5 fs	3.8−7.8 fs	3−3.8 fs	div.	div.	div.
PBE0	$> 5.10^{-5}$	13.1−14.7 fs	6.3−10.2 fs	3.2−5.5 fs	div.	div.	div.	div.

Finally, we turn to the effect of the XC functional. The ε_0 parameters, which determine the energy level of the continuum depend on the MO eigenvalues and hence on the chosen XC fuctional. Here, we consider four different flavors of functionals, namely the Local Density Approximation[105] (VWN), the Generalized Gradient Approximation[106] (PBE), the global hybrid[108] (PBE0) and the range separated[107] (LCPBE) functionals. ε_0 is set by Eq. (8) to 0.10, 0.098, 0.07 and 0 Ha for VWN, PBE, PBE0 and LCPBE, respectively. As expected, ε_0 is reduced with the inclusion of a higher fraction of exact exchange, resulting in a better

description of the energy outside the potential well. Note that for the long range corrected LCPBE functional, the correction is negligible. Figure 4 shows the deposit energies for each functional. The energy deposited at the moment of the collision depends weakly on the XC functional. This is reminiscent of previous comparisons made with the GGA and LDA functionals. This is likely due to the fact that energy deposition is the result of Coulomb scattering, for which exchange-correlation effects are negligible. However, the use of the functional LCPBE shows a significant stabilisation of the energy gap compared to that obtained with the functional PBE. The energy difference $E_{PBE-LCPBE}$ is about 190 kcal.mol^{-1}. This can be explained by the fact that the energies of the MOs depend on the functional used. In fact, the non-bounding MOs, calculated from the functional PBE0 or LCPBE, are higher in energy than those calculated with PBE or VWN. However, the distribution of excited electrons in these MOs remains globally unchanged from one functional to another, so there is a greater energy deposition for PBE0 and LCPBE than for PBE and VWN functionals.

If we consider the effects of functionals on other properties, such as the variation of atomic charges or the amount of electrons absorbed by the CAP, their effects seem negligible (Table 3). The same conclusion is drawn when we set the functional and vary the strength of the CAP with different values of γ_0.

Table 3: El_{abs} the number of absorbed electrons, and the root mean square deviation of the atomic charge for oxygen and hydrogen atoms, $H_{(1)}$ et $H_{(2)}$, in water molecule after irradiation

	RMSD					RMSD			
	PBE	VWN	PBE0	LCPBE	γ_0	0.025	0.05	0.1	0.2
O	0.000	0.012	0.020	0.020	O	0.000	0.022	0.023	0.024
$H_{(1)}$	0.000	0.006	0.010	0.011	$H_{(1)}$	0.000	0.013	0.015	0.017
$H_{(2)}$	0.000	0.006	0.010	0.011	$H_{(2)}$	0.000	0.013	0.015	0.017
El_{abs}	0.64	0.63	0.68	0.74					

Knowing that the O-H vibration mode is the fastest in a water molecule and that its frequency is about 0.1 fs^{-1}, the fixed nuclei approximation is no longer valid beyond 10 fs

of simulation. With the addition of a CAP, the stabilisation of the energy E_d should take place in this time interval. Calculating the gradient ∇E_d gives us information about the simulation duration needed to stabilize the energy. Table 2 summarizes all the time intervals during which the energy is stabilized. If the coefficient γ_0 is 0.025 Ha, the electron lifetimes are too long for the simulation time and stability is not achieved. For values of γ_0 higher than 0.2 Ha, unphysical self-ionisation phenomena occur, which prevent energy stabilisation.

In the case of the water molecule, a γ_0 value of 0.1 Ha, combined with a ξ value of 0.05 Ha^{-1} with a total propagation time of 7 fs seems to be a reasonable choice of parameters.

In summary, we have explored the use of energy CAP to simulate ion-collisions through RT-TD-ADFT simulations. Provided a careful parameter tuning is done, such CAP is suitable for such simulations. Interestingly the XC functional doesn't seem to have a strong effect

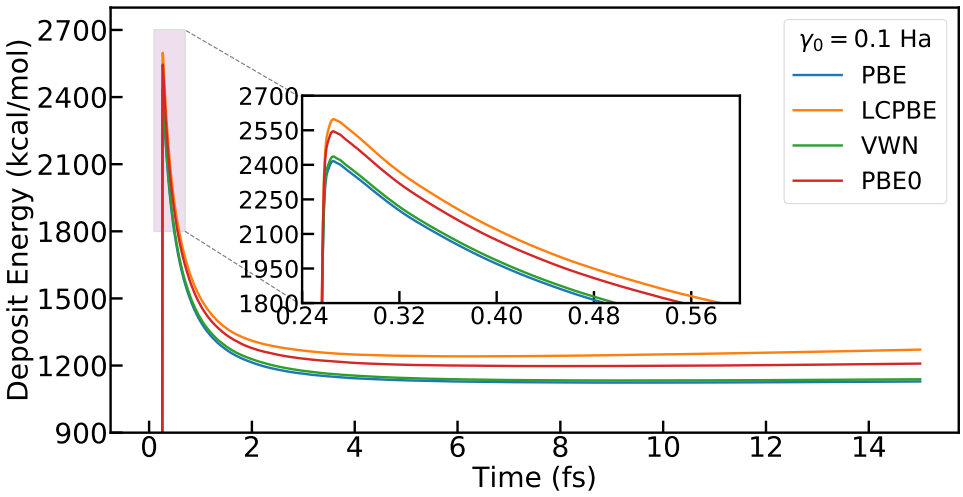

Figure 4: Deposit energy as a function of time at the RT-TD-ADFT level, using PBE (blue), LCPBE (orange), VWN (green) and PBE0 (red) functionals. The value of γ_0 is assigned to 0.1 Ha while ξ is fixed at 0.05 Ha^{-1}

TBP and $Pu(TBP)_2(NO_3)_4$ targets

The CAP parameters were determined using the same protocol as described above for alpha particle irradiation of TBP and $Pu(NO_3)_4(TBP)_2$. Table 4gathers the time periods following

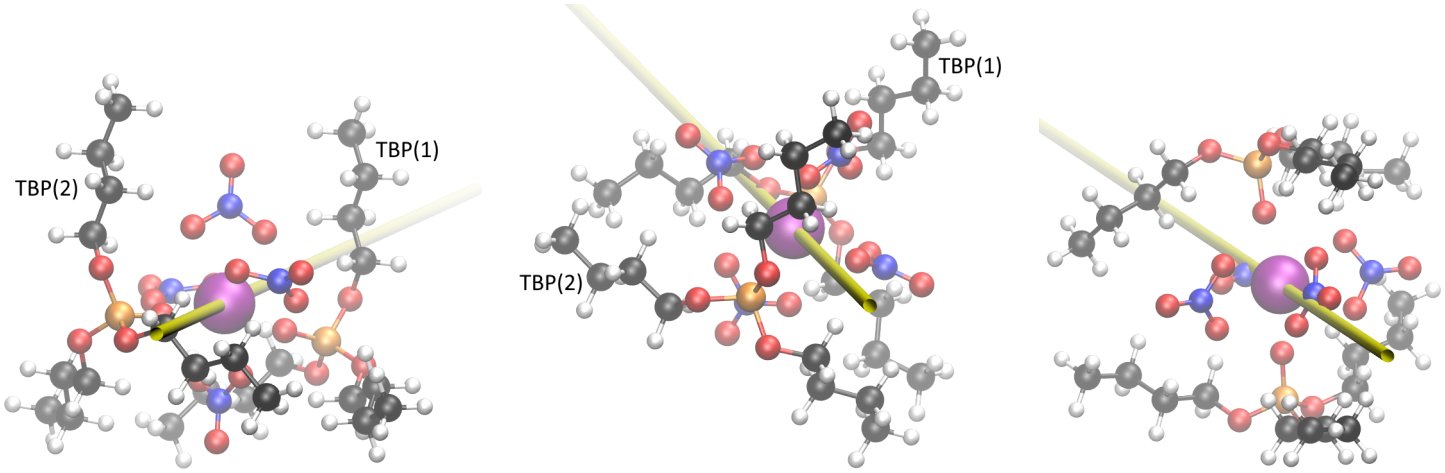

Figure 5: Visualisation of the trajectories A, B and C

the TBP irradiation, for which the energy stability is reached for a series of γ_0 values with a constant parameter ξ at 0.05 Ha^{-1}. For TBP, energy stabilization is achieved in less than 10 fs when γ_0 is between 0.4 and 0.8 Ha, but with a very limited time scale. To ensure the absorption of higher energy electrons without the risk of unphysical phenomena, a value of γ_0 lower than that announced will be taken. In the case of a simulation aiming at the total number of ejected electrons, a longer simulation time would be preferable.

The set of trajectory propagation vectors was defined from an orthonormal coordinate system, constructed from the coordinates of the atoms in $Pu(NO_3)_4(TBP)_2$. The origin of the frame is placed on the plutonium atom, which is approximately at the centre of mass of the system. The geometry of the complex $Pu(NO_3)_4(TBP)_2$ has an approximate C_4 symmetry along the x axis and 49 trajectories are extracted from a quarter sphere (figure 6). They all pass through the plutonium atom.

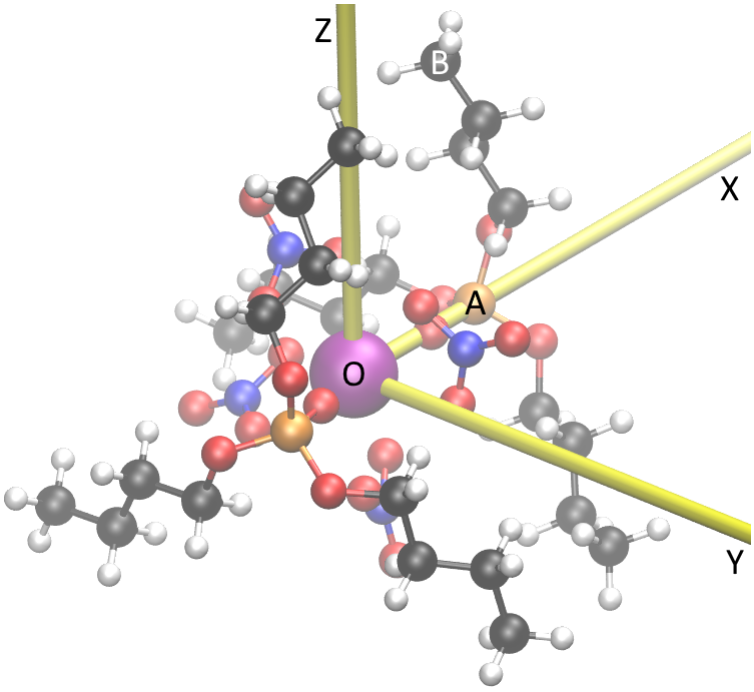

Figure 6: Orthonormal coordinate system (O,$\hat{x}$,$\hat{y}$) in yellow, made from the coordinates of the atoms in $Pu(NO_3)_4(TBP)_2$

Figure 7 shows the corresponding deposit energies for an isolated TBP molecule. The deposit energies are in the range [90; 1,007] kcal/mol for a 5.1 MeV alpha particle, while they are in the range [223; 4,968] kcal/mol for a 0.5 MeV alpha particle, which is around the Bragg peak in organic phase[114,115].

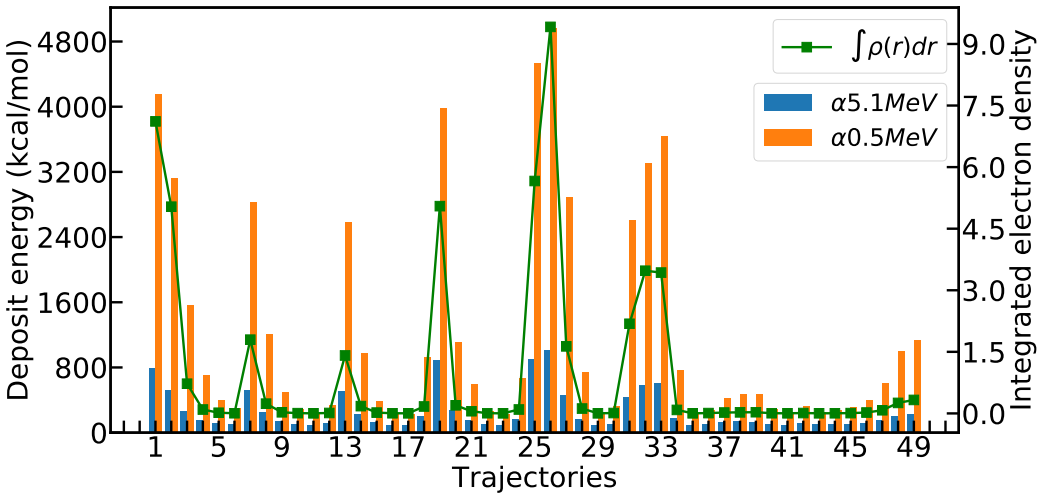

Figure 7: Deposit energy calculated for the 49 trajectories with corresponding electron density crossed by a 5.1 and 0.5 MeV projectile that interacts with a TBP target

TPB

Due to electrostatic interactions with the electron density and the high probability of ionization, new electronic states or intramolecular charge transfers are expected. To account for these phenomena, the evolution of the atomic charges of TBP is summed by splitting the molecule into four residues, the highly polar phosphate group (PO_4) and the three alkyl chains ($C_4H_9(1)$, $C_4H_9(2)$ and $C_4H_9(3)$). According to the residue labels in $Pu(TBP)_{25}NO_3)_4$ (section **??**), we work with TBP(2) in this part.

The charge variation profile depends on the type of residue crossed along the trajectory. Among the 49 trajectories, four representative profiles for charge variation can be distinguished. They correspond to the passage alternatively through an alkyl chain, nitrate ions or phosphate groups. An example is presented for the trajectory A shown in figure 5, the charges are plotted in Figure 8 (1). Trajectory vectors, cartesian coordinates of the complex, all the graph data and a python script to generate them are available in the Supporting Information (S.I.). During the passage of the alpha particle, which occurs at 0.22 fs, the relative charge of $C_4H_9(1)$ fragment drops to -0.24 due to the electrostatic attraction of the helium nuclei. This process goes hand in hand with the positive charge values of the other

residues. Then the electron density relaxes and the charge of the phosphate group reaches 0.08 above its initial value. This electronic density perturbation is well known in the literature from the Barkas effect[116,117], which demonstrated the polarisation of the electronic cloud when charged projectiles interact with a molecular target. We show that this effect is effectively captured by RT-TD-DFT[118].

After a relaxation time of 0.4 fs, the atomic charge of the group $C_4H_9(1)$ increases again before stabilizing around 0.16. At the same time, we observe a progressive increases of the charges of $C_4H_9(2)$ and $C_4H_9(3)$. These charge transfers come from all the alkyl chains and seem to stabilize the atomic charge of the phosphate group.

This is confirmed when a simulation is performed with a 0.5 MeV alpha particle (Figure 8 (2)). As stated above, in the kinetic energy range [0.5, 5.1] MeV, a decrease in velocity results in an increase in the amount of energy deposited, 248 kcal/mol for a 5.1 MeV and 2,831 kcal/mol for a 0.5 MeV kinetic energy projectile, as well as the number of electrons ejected. As a result, the variations of the fragment charges are amplified. They reveal that electrons of the phosphate groups and of $C_4H_9(2)$ are emitted after the relaxation time. From 1.3 fs an important charge transfer of $C_4H_9(1)$, $C_4H_9(2)$ and $C_4H_9(3)$ stabilises quickly the charge of PO_4 between 0.24 and 0.55. A new charge transfer occurs between the alkyl chains during this time of the simulation.

Table 4: Periods of time following the irradiation of the TBP, for which the energy stability is reached and between -5.10^{-5} and $+5.10^{-5}$ kcal.mol^{-1}. The simulations were performed at the RT-TD-ADFT level, with the functional PBE, the atomic base cc-PVTZ, and the auxiliary base GEN-A2*.

	$\xi = 0.05$							
γ_0	0.025	0.05	0.1	0.2	0.4	0.8	2.0	3.0
$\tau(E_{\text{stab}})$	no stab.	no stab.	no stab.	no stab.	$7.1 - 7.5$ fs	$3.3 - 3.4$ fs	div.	div.

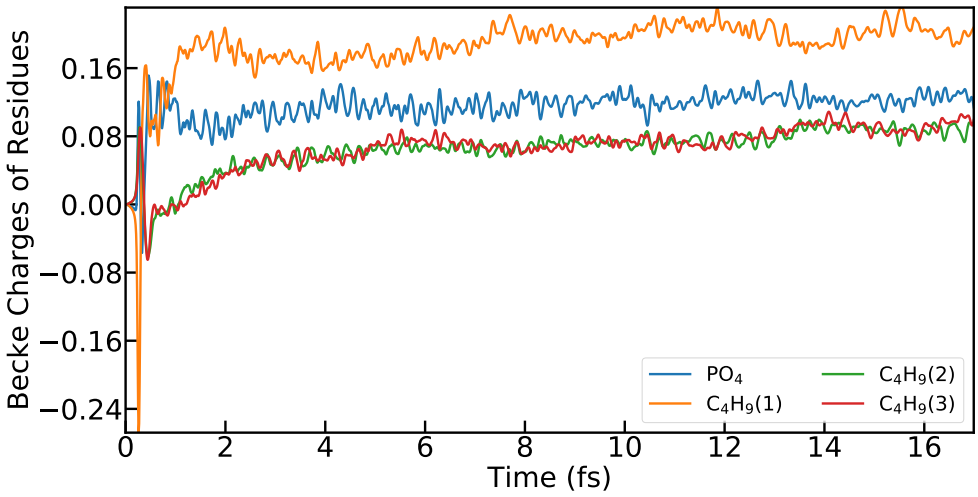

(1)

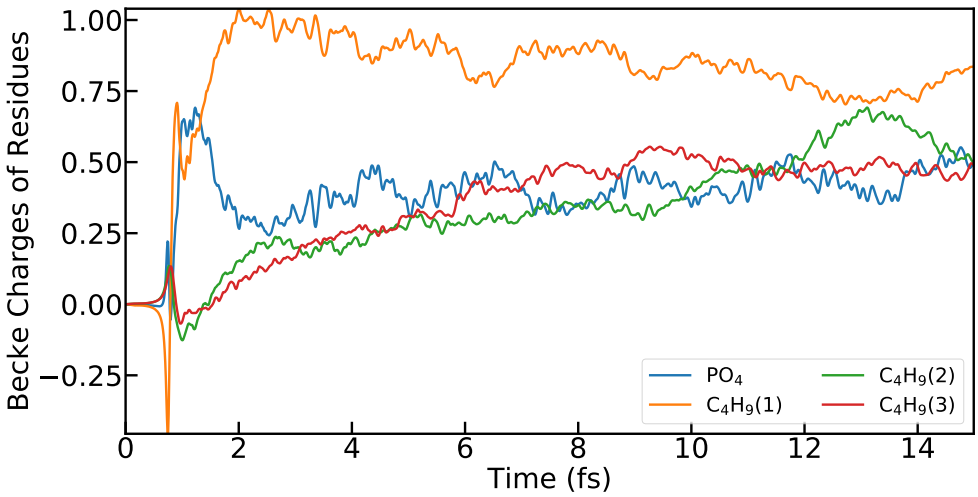

(2)

Figure 8: Residues charge variation in free TBP for the trajectory A. (1) 5.1 MeV; (2) 0.5 MeV alpha particle kinetic energy

$\mathbf{Pu(NO_3)_4(TBP)_2}$

To analyze the variations of atomic charges in the $Pu(NO_3)_4(TBP)_2$ complex, the latter is divided into seven residues: the plutonium atom Pu, the TBP(1) and TBP (2) molecules, and the four nitrate ions labeled $NO_3(1)$, $NO_3(2)$, $NO_3(3)$ and $NO_3(4)$. The TBP described in the previous part corresponds to the residue TBP(2).

The variations of fragment charges for trajectory A are represented in figure 9. A higher

charge accumulation is observed in TBP(1) after the initial electronic relaxation compared to TBP(2). The total atomic charge of TBP(1) stabilizes around -0.20. We also note an increase in the charges of the nitrate groups at the same time, with the appearance of charge transfers from 7 fs. The charges of the plutonium atom and TBP(2) remain almost unchanged during the simulation. The charge distributions in the phosphate group and the alkyl chains of TBP(2) show the same orders of magnitude to those of the isolated TBP molecule. However, intramolecular charge transfers are completely absent.

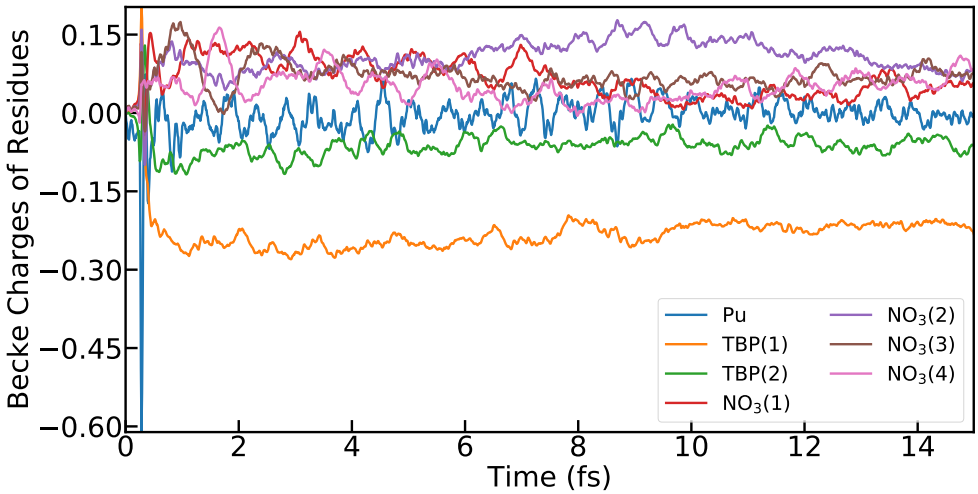

Figure 9: Residues charge variation in $Pu(NO_3)_4(TBP)_2$ for the trajectory A. Alpha particle kinetic energy of 5.1 MeV

In the case of trajectory B (Figure 5), the projectile passes through the electron densities of both TBPs. The collision occurs first with TBP(2) and then with TBP(1). The atomic charge of TBP(1) then decreases rapidly, following the relaxation period of the system, to stabilize between -0.33 and -0.20. In parallel, we observe an evolution of the TBP(2) charge into positive values, with a maximum at 0.17, before decreasing to its initial value after 12 fs of simulation. Analysis of the charges on the phosphate group of the butyl chains of TBP shows that the projectile interacts more strongly with TBP(2) than with TBP(1). The accumulation of charges in TBP(1) is due to the presence of the other ligands in the complex, since no similar atomic charge profile is found in the analyses of free TBP.

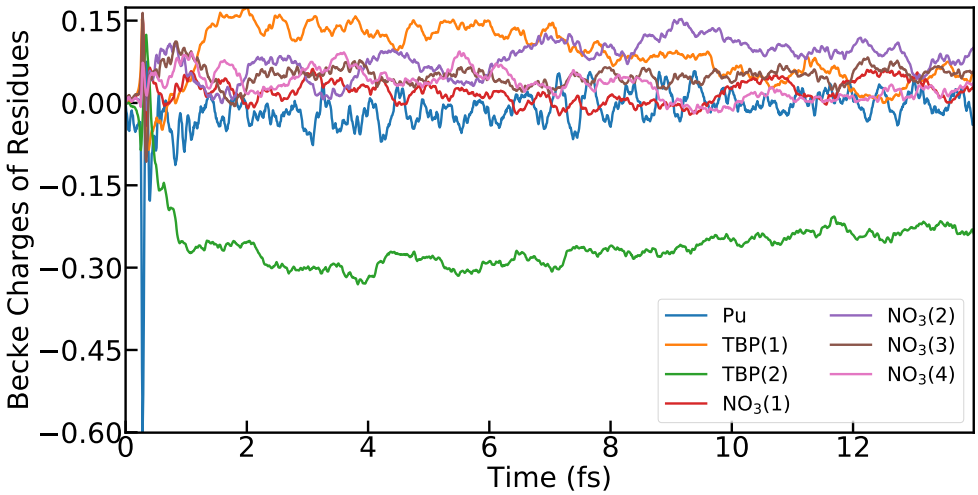

Figure 10: Residues charge variation in $Pu(NO_3)_4(TBP)_2$ for the trajectory B. Alpha particle kinetic energy of 5.1 MeV

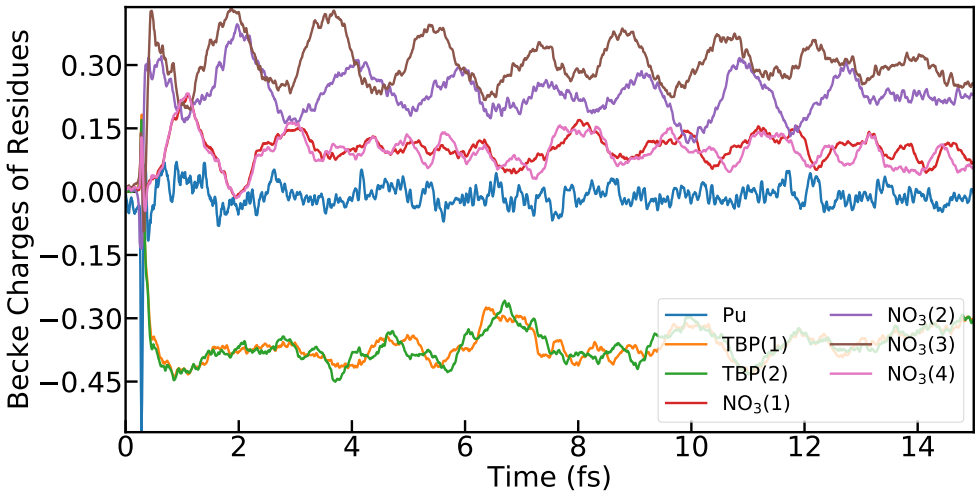

Figure 11: Residues charge variation in $Pu(NO_3)_4(TBP)_2$ for the trajectory C. Alpha particle kinetic energy of 5.1 MeV

The influence of the ligands on the TBP molecules is evident from the analysis of trajectory C (Figure 5). In this case, the projectile passes through the regions of electronic density corresponding to the location of the nitrates. Their atomic charges are all positive after relaxation, and the charge transfer occurs periodically during the simulation. Although the interaction between alpha particle and TBP interaction is extremely weak, there is a sudden decrease in their atomic charges, which is not observed for an isolated TBP molecule.

Analysis of the TBP(2) residues shows that the charge accumulation is distributed over the three alkyl chains. However, these observations should be taken with a critical eye because they do not account for ionization effects in the system. It is therefore possible to consider other intra- and inter-molecular charge migration phenomena.

Conclusion

In this work, we have shown that RT-DT-ADFT method can be used to reproduce the interaction of an alpha particle with a free organic molecule such as TBP, and a complex formed with a plutonium cation, TBP and nitrate molecules. We have demonstrated that complexation changes the response of the electron cloud to the perturbation of the charged projectile. This is due to the presence of the other ligands. In particular, an important charge accumulation occurs on TBP when it interacts weakly with the alpha particle.

We also investigated the use of CAP in energy space to absorb electrons ejected during irradiation by swift ions. A detailed analysis of the choice of the CAP parameters on the water molecule reveals the occurrence of unphysical phenomena when the CAP strength exceed a threshold value. It reveals that a set of parameters defines a period of time during which the total energy is stabilized, and so the best duration of a simulation.

Application of CAP on Hamiltonian for the irradiation of a water molecule or TBP absorbs less than one electron along a 15 fs electron dynamics, using a 5.1 MeV projectile. In the case of a less energetic alpha particle, around the Bragg peak, the number of ejected electrons increases to 2, making the application of CAP essential to avoid self-ionization effects.

To conclude, we demonstrate that a CAP in energy space can be used as a good alternative solution of real space CAP when the choice of a large basis set cannot be applied of the system.

Acknowledgement

We are grateful to GENCI for providing us with generous computational ressources (project number A0120806830)

Conflict of Interest: The authors declare no competing interests

References

(1) Allisy, A. Henri Becquerel: the discovery of radioactivity. *Radiation protection dosimetry* **1996**, *68*, 3–10.

(2) Pasachoff, N. *Marie Curie: And the science of radioactivity*; Oxford University Press, 1996.

(3) Arumainayagam, C. R.; Garrod, R. T.; Boyer, M. C.; Hay, A. K.; Bao, S. T.; Campbell, J. S.; Wang, J.; Nowak, C. M.; Arumainayagam, M. R.; Hodge, P. J. Extraterrestrial prebiotic molecules: photochemistry vs. radiation chemistry of interstellar ices. *Chemical Society Reviews* **2019**, *48*, 2293–2314.

(4) Kumar, K. P.; Sundaram, G. S.; Venkatesh, S.; Gandhiraj, R.; Thiruvengadathan, R. A Monte Carlo simulation study of L-band emission upon gamma radiolysis of water. *Radiation Physics and Chemistry* **2023**, 110883.

(5) Hughes, J. R.; Parsons, J. L. FLASH radiotherapy: current knowledge and future insights using proton-beam therapy. *International journal of molecular sciences* **2020**, *21*, 6492.

(6) Brenner, D. J.; Hall, E. J. Secondary neutrons in clinical proton radiotherapy: a charged issue. *Radiotherapy and Oncology* **2008**, *86*, 165–170.

(7) da Silva Aquino, K. A. Sterilization by gamma irradiation. *Gamma radiation* **2012**, *9*, 172–202.

(8) Krishnamurthy, M.; Sipahimalani, A. Radiolytic degradation of TBP-HNO 3 system: Gas chromatographic determination of radiation chemical yields of n-Butanol and nitrobutane. *Journal of radioanalytical and nuclear chemistry* **1995**, *199*, 197–206.

(9) Lesage, D.; Virelizier, H.; Jankowski, C. K.; Tabet, J. C. Identification of minor products obtained during radiolysis of tributylphosphate (TBP). *Spectroscopy* **1997**, *13*, 275–290.

(10) Parikh, K.; Pathak, P.; Misra, S.; Tripathi, S.; Dakshinamoorthy, A.; Manchanda, V. Radiolytic degradation studies on N, N-dihexyloctanamide (DHOA) under PUREX process conditions. *Solvent Extraction and Ion Exchange* **2009**, *27*, 244–257.

(11) Wang, F.; Horne, G. P.; Pernot, P.; Archirel, P.; Mostafavi, M. Picosecond Pulse Radiolysis Study on the Radiation-Induced Reactions in Neat Tributyl Phosphate. *122*, 7134–7142, Publisher: American Chemical Society.

(12) Ma, J.; Denisov, S. A.; Marignier, J.-L.; Pernot, P.; Adhikary, A.; Seki, S.; Mostafavi, M. Ultrafast Electron Attachment and Hole Transfer Following Ionizing Radiation of Aqueous Uridine Monophosphate. *9*, 5105–5109, Publisher: American Chemical Society.

(13) Bahry, T.; Denisov, S. A.; Moisy, P.; Ma, J.; Mostafavi, M. Real-Time Observation of Solvation Dynamics of Electron in Actinide Extraction Binary Solutions of Water and n-Tributyl Phosphate. *125*, 3843–3849, Publisher: American Chemical Society.

(14) Lara-Astiaso, M.; Galli, M.; Trabattoni, A.; Palacios, A.; Ayuso, D.; Frassetto, F.; Poletto, L.; De Camillis, S.; Greenwood, J.; Decleva, P., et al. Attosecond pump–probe spectroscopy of charge dynamics in tryptophan. *The journal of physical chemistry letters* **2018**, *9*, 4570–4577.

(15) Plésiat, E.; Lara-Astiaso, M.; Decleva, P.; Palacios, A.; Martín, F. Real-time imag-

ing of ultrafast charge dynamics in tetrafluoromethane from attosecond pump-probe photoelectron spectroscopy. *Chemistry–A European Journal* **2018**, *24*, 12061–12070.

(16) Tandiana, R.; Brun, E.; Sicard-Roselli, C.; Domin, D.; Van-Oanh, N.-T.; Clavaguéra, C. Probing the structural properties of the water solvation shell around gold nanoparticles: A computational study. *154*, 044706, Publisher: American Institute of Physics.

(17) Omar, K. A.; Hasnaoui, K.; de la Lande, A. First-Principles Simulations of Biological Molecules Subjected to Ionizing Radiation. *72*, 445–465, _eprint: https://doi.org/10.1146/annurev-physchem-101419-013639.

(18) Alvarez-Ibarra, A.; Parise, A.; Hasnaoui, K.; Lande, A. d. l. The physical stage of radiolysis of solvated DNA by high-energy-transfer particles: insights from new first principles simulations. *22*, 7747–7758, Publisher: Royal Society of Chemistry.

(19) Runge, E.; Gross, E. K. U. Density-Functional Theory for Time-Dependent Systems. *52*, 997–1000, Publisher: American Physical Society.

(20) Theilhaber, J. Ab initio simulations of sodium using time-dependent density-functional theory. *Physical Review B* **1992**, *46*, 12990.

(21) Yabana, K.; Bertsch, G. Time-dependent local-density approximation in real time. *Physical Review B* **1996**, *54*, 4484.

(22) Calvayrac, F.; Reinhard, P.; Suraud, E. Nonlinear plasmon response in highly excited metallic clusters. *Physical Review B* **1995**, *52*, R17056.

(23) Casida, M. E. *Recent Advances In Density Functional Methods: (Part I)*; World Scientific, 1995; pp 155–192.

(24) Tandiana, R.; Clavaguéra, C.; Hasnaoui, K.; Pedroza-Montero, J. N.; de La Lande, A.

Reliability and performances of real-time time-dependent auxiliary density functional theory. *Theoretical Chemistry Accounts* **2021**, *140*, 126.

(25) Köster, A. M. Hermite Gaussian auxiliary functions for the variational fitting of the Coulomb potential in density functional methods. *The Journal of chemical physics* **2003**, *118*, 9943–9951.

(26) Sharma, V.; Fernández-Serra, M. Proton-transfer dynamics in ionized water chains using real-time time-dependent density functional theory. *2*, 043082, Publisher: American Physical Society.

(27) Cai, Z.; Chen, S.; Wang, L.-W. Dissociation path competition of radiolysis ionization-induced molecule damage under electron beam illumination. *10*, 10706–10715, Publisher: Royal Society of Chemistry.

(28) Deng, Z.-Y.; Hu, Z.; Feng, H.-J. Ultrafast nonadiabatic dynamics of λ-DNA upon low energy proton irradiation. *120*, 043702, Publisher: American Institute of Physics.

(29) Miyamoto, Y.; Rubio, A. Application of the Real-Time Time-Dependent Density Functional Theory to Excited-State Dynamics of Molecules and 2D Materials. *87*, 041016, Publisher: The Physical Society of Japan.

(30) Yost, D. C.; Yao, Y.; Kanai, Y. Examining real-time TDDFT non-equilibrium simulations for the calculation of electronic stopping power. *96*, 115134.

(31) Reeves, K. G.; Yao, Y.; Kanai, Y. Electronic stopping power in liquid water for protons and \ensuremath{\alpha} particles from first principles. *94*, 041108, Publisher: American Physical Society.

(32) Yost, D. C.; Yao, Y.; Kanai, Y. Examining real-time time-dependent density functional theory nonequilibrium simulations for the calculation of electronic stopping power. *96*, 115134, Publisher: American Physical Society.

(33) Maliyov, I.; Crocombette, J.-P.; Bruneval, F. Quantitative electronic stopping power from localized basis set. *101*, 035136, Publisher: American Physical Society.

(34) Bi, G.; Kang, J.; Wang, L.-W. High velocity proton collision with liquid lithium: a time dependent density functional theory study. *19*, 9053–9058, Publisher: Royal Society of Chemistry.

(35) Lacombe, L.; Huong Mai Dinh, P.; Reinhard, P.-G.; Suraud, E.; Sanche, L. Rare reaction channels in real-time time-dependent density functional theory: the test case of electron attachment. *69*, 195.

(36) Fuks, J. I.; Lacombe, L.; Nielsen, S. E.; Maitra, N. T. Exploring non-adiabatic approximations to the exchange–correlation functional of TDDFT. *Physical Chemistry Chemical Physics* **2018**, *20*, 26145–26160.

(37) de la Lande, A. Femtosecond responses of hydrated DNA irradiated by ionizing rays focus on the sugar-phosphate part. *140*, 77.

(38) Kononov, A.; Lee, C.-W.; dos Santos, T. P.; Robinson, B.; Yao, Y.; Yao, Y.; Andrade, X.; Baczewski, A. D.; Constantinescu, E.; Correa, A. A., et al. Electron dynamics in extended systems within real-time time-dependent density-functional theory. *MRS Communications* **2022**, *12*, 1002–1014.

(39) Neuhasuer, D.; Baer, M. The time-dependent Schrödinger equation: Application of absorbing boundary conditions. *90*, 4351–4355, Publisher: American Institute of Physics.

(40) Baer, M.; Neuhauser, D.; Oreg, Y. A new accurate (time-independent) method for treating reactive collisions: conversion of a scattering problem into a bound problem. *86*, 1721–1727, Publisher: Royal Society of Chemistry.

(41) Neuhauser, D.; Baer, M.; Kouri, D. J. The application of optical potentials for reactive scattering: A case study. *93*, 2499–2505, Publisher: American Institute of Physics.

(42) Bisseling, R. H.; Kosloff, R.; Manz, J. Dynamics of hyperspherical and local mode resonance decay studied by time dependent wave packet propagation. *83*, 993–1004, Publisher: American Institute of Physics.

(43) Vibok, A.; Balint-Kurti, G. G. Parametrization of complex absorbing potentials for time-dependent quantum dynamics. *96*, 8712–8719.

(44) Riss, U. V.; Meyer, H.-D. Calculation of resonance energies and widths using the complex absorbing potential method. *26*, 4503.

(45) Kononov, A.; Lee, C.-W.; dos Santos, T. P.; Robinson, B.; Yao, Y.; Yao, Y.; Andrade, X.; Baczewski, A. D.; Constantinescu, E.; Correa, A. A.; Kanai, Y.; Modine, N.; Schleife, A. Electron dynamics in extended systems within real-time time-dependent density-functional theory. *12*, 1002–1014.

(46) Sissay, A.; Abanador, P.; Mauger, F.; Gaarde, M.; Schafer, K. J.; Lopata, K. Angle-dependent strong-field molecular ionization rates with tuned range-separated time-dependent density functional theory. *145*, 094105, Publisher: American Institute of Physics.

(47) De Giovannini, U.; Hübener, H.; Rubio, A. A First-Principles Time-Dependent Density Functional Theory Framework for Spin and Time-Resolved Angular-Resolved Photoelectron Spectroscopy in Periodic Systems. *13*, 265–273, Publisher: American Chemical Society.

(48) Aguilar-Galindo, F.; Borisov, A. G.; Díaz-Tendero, S. Ultrafast Dynamics of Electronic Resonances in Molecules Adsorbed on Metal Surfaces: A Wave Packet Propagation Approach. *17*, 639–654, Publisher: American Chemical Society.

(49) Hoerner, P.; Lee, M. K.; Schlegel, H. B. Angular dependence of strong field ionization of N2 by time-dependent configuration interaction using density functional theory

and the Tamm-Dancoff approximation. *151*, 054102, Publisher: American Institute of Physics.

(50) De Giovannini, U.; Hübener, H.; Rubio, A. A first principles TDDFT framework for spin and time-resolved ARPES in periodic systems. *13*, 265–273.

(51) Meng, Q.; Schröder, M.; Meyer, H.-D. High-Dimensional Quantum Dynamics Study on Excitation-Specific Surface Scattering Including Lattice Effects of a Five-Atom Surface Cell. *17*, 2702–2713, Publisher: American Chemical Society.

(52) Ruberti, M.; Decleva, P.; Averbukh, V. Full Ab Initio Many-Electron Simulation of Attosecond Molecular Pump–Probe Spectroscopy. *14*, 4991–5000, Publisher: American Chemical Society.

(53) Ghosh, S.; Sahoo, T.; Baer, M.; Adhikari, S. Charge Transfer Processes for H + H2+ Reaction Employing Coupled 3D Wavepacket Approach on Beyond Born–Oppenheimer Based Ab Initio Constructed Diabatic Potential Energy Surfaces. *125*, 731–745, Publisher: American Chemical Society.

(54) Kononov, A.; Lee, C.-W.; dos Santos, T. P.; Robinson, B.; Yao, Y.; Yao, Y.; Andrade, X.; Baczewski, A. D.; Constantinescu, E.; Correa, A. A.; Kanai, Y.; Modine, N.; Schleife, A. Electron dynamics in extended systems within real-time time-dependent density-functional theory. *12*, 1002–1014.

(55) Davis, J. U. J.; Phung, Q. M.; Yanai, T.; Ehara, M.; Sommerfeld, T. Lifetimes of Be32– and Mg32– Cluster Dianions. *125*, 3579–3588, Publisher: American Chemical Society.

(56) Lande, A. d. l.; Denisov, S.; Mostafavi, M. The mystery of sub-picosecond charge transfer following irradiation of hydrated uridine monophosphate. *23*, 21148–21162, Publisher: Royal Society of Chemistry.

(57) Davidsson, E.; Kowalewski, M. Simulating photodissociation reactions in bad cavities with the Lindblad equation. *153*, 234304, Publisher: American Institute of Physics.

(58) Naskar, K.; Ghosh, S.; Adhikari, S. Accurate Calculation of Rate Constant and Isotope Effect for the F + H2 Reaction by the Coupled 3D Time-Dependent Wave Packet Method on the Newly Constructed Ab Initio Ground Potential Energy Surface. *126*, 3311–3328, Publisher: American Chemical Society.

(59) Sun, Z.; Wang, C.; Zhao, W.; Yang, C. Geometric phase effects on photodissociation dynamics of diatomics. *149*, 224307, Publisher: American Institute of Physics.

(60) Li, J.; Zhao, B.; Xie, D.; Guo, H. Advances and New Challenges to Bimolecular Reaction Dynamics Theory. *11*, 8844–8860, Publisher: American Chemical Society.

(61) Epifanovsky, E.; Gilbert, A. T.; Feng, X.; Lee, J.; Mao, Y.; Mardirossian, N.; Pokhilko, P.; White, A. F.; Coons, M. P.; Dempwolff, A. L., et al. Software for the frontiers of quantum chemistry: An overview of developments in the Q-Chem 5 package. *155*, 084801, Publisher: American Institute of Physics.

(62) Skomorowski, W.; Krylov, A. I. Real and Imaginary Excitons: Making Sense of Resonance Wave Functions by Using Reduced State and Transition Density Matrices. *9*, 4101–4108, Publisher: American Chemical Society.

(63) Krause, P.; Sonk, J. A.; Schlegel, H. B. Strong field ionization rates simulated with time-dependent configuration interaction and an absorbing potential. *140*, 174113, Publisher: American Institute of Physics.

(64) Phung, Q. M.; Komori, Y.; Yanai, T.; Sommerfeld, T.; Ehara, M. Combination of a Voronoi-Type Complex Absorbing Potential with the XMS-CASPT2 Method and Pilot Applications. *16*, 2606–2616, Publisher: American Chemical Society.

(65) Das, S.; Sajeev, Y.; Samanta, K. An Electron Propagator Approach Based on a Multiconfigurational Reference State for the Investigation of Negative-Ion Resonances Using a Complex Absorbing Potential Method. *16*, 5024–5034, Publisher: American Chemical Society.

(66) Thodika, M.; Matsika, S. Projected Complex Absorbing Potential Multireference Configuration Interaction Approach for Shape and Feshbach Resonances. *18*, 3377–3390, Publisher: American Chemical Society.

(67) Kumar, R.; Ghosh, A.; Vaval, N. Decay Processes in Cationic Alkali Metals in Microsolvated Clusters: A Complex Absorbing Potential Based Equation-of-Motion Coupled Cluster Investigation. *18*, 807–816, Publisher: American Chemical Society.

(68) Benda, Z.; Jagau, T.-C. Understanding Processes Following Resonant Electron Attachment: Minimum-Energy Crossing Points between Anionic and Neutral Potential Energy Surfaces. *14*, 4216–4223, Publisher: American Chemical Society.

(69) Benda, Z.; Rickmeyer, K.; Jagau, T.-C. Structure Optimization of Temporary Anions. *14*, 3468–3478, Publisher: American Chemical Society.

(70) Thodika, M.; Fennimore, M.; Karsili, T. N. V.; Matsika, S. Comparative study of methodologies for calculating metastable states of small to medium-sized molecules. *151*, 244104, Publisher: American Institute of Physics.

(71) Gayvert, J. R.; Bravaya, K. B. Projected CAP-EOM-CCSD method for electronic resonances. *156*, 094108, Publisher: American Institute of Physics.

(72) Gayvert, J. R.; Bravaya, K. B. Application of Box and Voronoi CAPs for Metastable Electronic States in Molecular Clusters. *126*, 5070–5078, Publisher: American Chemical Society.

(73) Bhattacharya, D.; Ben-Asher, A.; Haritan, I.; Pawlak, M.; Landau, A.; Moiseyev, N. Polyatomic ab Initio Complex Potential Energy Surfaces: Illustration of Ultracold Collisions. *13*, 1682–1690, Publisher: American Chemical Society.

(74) Jagau, T.-C. Non-iterative triple excitations in equation-of-motion coupled-cluster theory for electron attachment with applications to bound and temporary anions. *148*, 024104, Publisher: American Institute of Physics.

(75) Mukherjee, M.; Ragesh Kumar, T. P.; Ranković, M.; Nag, P.; Fedor, J.; Krylov, A. I. Spectroscopic signatures of states in the continuum characterized by a joint experimental and theoretical study of pyrrole. *157*, 204305, Publisher: American Institute of Physics.

(76) Papp, D.; Császár, A. G.; Yamanouchi, K.; Szidarovszky, T. Rovibrational Resonances in H2He+. *14*, 1523–1533, Publisher: American Chemical Society.

(77) Kanazawa, Y.; Ehara, M.; Sommerfeld, T. Low-Lying π^* Resonances of Standard and Rare DNA and RNA Bases Studied by the Projected CAP/SAC–CI Method. *120*, 1545–1553, Publisher: American Chemical Society.

(78) Sajeev, Y.; Thodika, M.; Matsika, S. A Unique QP Partitioning and Siegert Width Using Real-Valued Continuum-Remover Potential. *18*, 2863–2874, Publisher: American Chemical Society.

(79) Sommerfeld, T.; Melugin, J. B.; Ehara, M. Temporary Anion States of Ethene Interacting with Single Molecules of Methane, Ethane, and Water. *122*, 2580–2586, Publisher: American Chemical Society.

(80) Simkó, I.; Szidarovszky, T.; Császár, A. G. Toward Automated Variational Computation of Rovibrational Resonances, Including a Case Study of the H2 Dimer. *15*, 4156–4169, Publisher: American Chemical Society.

(81) Sommerfeld, T.; Melugin, J. B.; Hamal, P.; Ehara, M. Resonance Energies and Lifetimes from the Analytic Continuation of the Coupling Constant Method: Robust Algorithms and a Critical Analysis. *13*, 2550–2560, Publisher: American Chemical Society.

(82) Sulzer, D.; Yasuda, K. Resonance State Method for Electron Injection in Dye Sensitized Solar Cells. *14*, 5090–5104, Publisher: American Chemical Society.

(83) Dempwolff, A. L.; Belogolova, A. M.; Sommerfeld, T.; Trofimov, A. B.; Dreuw, A. CAP/EA-ADC method for metastable anions: Computational aspects and application to π^* resonances of norbornadiene and 1,4-cyclohexadiene. *155*, 054103, Publisher: American Institute of Physics.

(84) Zhu, Y.; Herbert, J. M. High harmonic spectra computed using time-dependent Kohn–Sham theory with Gaussian orbitals and a complex absorbing potential. *156*, 204123, Publisher: American Institute of Physics.

(85) White, A. F.; Heide, C. J.; Saalfrank, P.; Head-Gordon, M.; Luppi, E. Computation of high-harmonic generation spectra of the hydrogen molecule using time-dependent configuration-interaction. *114*, 947–956, Publisher: Taylor & Francis _eprint: https://doi.org/10.1080/00268976.2015.1119900.

(86) Witzorky, C.; Paramonov, G.; Bouakline, F.; Jaquet, R.; Saalfrank, P.; Klamroth, T. Gaussian-Type Orbital Calculations for High Harmonic Generation in Vibrating Molecules: Benchmarks for H2+. *17*, 7353–7365, Publisher: American Chemical Society.

(87) Benda, Z.; Jagau, T.-C. Locating Exceptional Points on Multidimensional Complex-Valued Potential Energy Surfaces. *9*, 6978–6984, Publisher: American Chemical Society.

(88) Parravicini, V.; Jagau, T.-C. Embedded equation-of-motion coupled-cluster theory for electronic excitation, ionisation, electron attachment, and electronic resonances. *119*, e1943029, Publisher: Taylor & Francis _eprint: https://doi.org/10.1080/00268976.2021.1943029.

(89) Lee, M. K.; Hoerner, P.; Li, W.; Schlegel, H. B. Effect of spin–orbit coupling on strong field ionization simulated with time-dependent configuration interaction. *153*, 244109, Publisher: American Institute of Physics.

(90) Parise, A.; Alvarez-Ibarra, A.; Wu, X.; Zhao, X.; Pilmé, J.; de la Lande, A. Quantum chemical topology of the electron localization function in the field of attosecond electron dynamics. *The Journal of Physical Chemistry Letters* **2018**, *9*, 844–850.

(91) Klinkusch, S.; Saalfrank, P.; Klamroth, T. Laser-induced electron dynamics including photoionization: A heuristic model within time-dependent configuration interaction theory. *131*, 114304, Publisher: American Institute of Physics.

(92) Niehaus, T. A.; Meziane, M.; Lepine, F.; Marciniak, A.; Yamazaki, K.; Kono, H. Pulse shape and molecular orientation determine the attosecond charge migration in Caffeine. *91*, 152.

(93) Fernando, R. G.; Balhoff, M. C.; Lopata, K. X-ray Absorption in Insulators with Non-Hermitian Real-Time Time-Dependent Density Functional Theory. *11*, 646–654, Publisher: American Chemical Society.

(94) Lopata, K.; Govind, N. Near and Above Ionization Electronic Excitations with Non-Hermitian Real-Time Time-Dependent Density Functional Theory. *9*, 4939–4946, Publisher: American Chemical Society.

(95) Sulka, M.; Cantrel, L.; Vallet, V. Theoretical study of plutonium (IV) complexes formed within the PUREX process: A proposal of a plutonium surrogate in fire conditions. *The Journal of Physical Chemistry A* **2014**, *118*, 10073–10080.

(96) Gopakumar, G.; Sreenivasulu, B.; Suresh, A.; Brahmmananda Rao, C.; Sivaraman, N.; Joseph, M.; Anoop, A. Complexation behavior of the tri-n-butyl phosphate ligand with Pu (IV) and Zr (IV): a computational study. *The Journal of Physical Chemistry A* **2016**, *120*, 4201–4210.

(97) Lanham, W.; Runion, T. *PUREX process for plutonium and uranium recovery*; 1949.

(98) DeMon2k, A. M. K.; Calaminici, P.; Casida, M. E.; Flores-Moreno, R.; Geudtner, G.; Goursot, A.; Heine, T.; Ipatov, A.; Janetzko, F.; Jorge, M. del Campo, Serguei Patchkovskii, J. *Ulises Reveles, Dennis R. Salahub, Alberto Vela, deMon developers* **2006**,

(99) Dunlap, B.; Connolly, J.; Sabin, J. On first-row diatomic molecules and local density models. *The Journal of Chemical Physics* **1979**, *71*, 4993–4999.

(100) Köster, A. M.; Reveles, J. U.; del Campo, J. M. Calculation of exchange-correlation potentials with auxiliary function densities. *The Journal of chemical physics* **2004**, *121*, 3417–3424.

(101) Tsuneda, T.; Song, J.-W.; Suzuki, S.; Hirao, K. On Koopmans' theorem in density functional theory. *The Journal of chemical physics* **2010**, *133*, 174101.

(102) Kar, R.; Song, J.-W.; Hirao, K. Long-range corrected functionals satisfy Koopmans' theorem: calculation of correlation and relaxation energies. *Journal of Computational Chemistry* **2013**, *34*, 958–964.

(103) Tsuneda, T.; Hirao, K. Long-range correction for density functional theory. *Wiley Interdisciplinary Reviews: Computational Molecular Science* **2014**, *4*, 375–390.

(104) Moritz, A.; Cao, X.; Dolg, M. Quasirelativistic energy-consistent 5f-in-core pseudopotentials for divalent and tetravalent actinide elements. *Theoretical Chemistry Accounts* **2007**, *118*, 845–854.

(105) Vosko, S. H.; Wilk, L.; Nusair, M. Accurate spin-dependent electron liquid correlation energies for local spin density calculations: a critical analysis. *Canadian Journal of physics* **1980**, *58*, 1200–1211.

(106) Perdew, J. P.; Burke, K.; Ernzerhof, M. Generalized gradient approximation made simple. *Physical review letters* **1996**, *77*, 3865.

(107) Iikura, H.; Tsuneda, T.; Yanai, T.; Hirao, K. A long-range correction scheme for generalized-gradient-approximation exchange functionals. *The Journal of Chemical Physics* **2001**, *115*, 3540–3544.

(108) Adamo, C.; Barone, V. Toward reliable density functional methods without adjustable parameters: The PBE0 model. *The Journal of chemical physics* **1999**, *110*, 6158–6170.

(109) Köster, A. M.; Del Campo, J. M.; Janetzko, F.; Zuniga-Gutierrez, B. A MinMax self-consistent-field approach for auxiliary density functional theory. *The Journal of chemical physics* **2009**, *130*, 114106.

(110) Yost, D. C.; Yao, Y.; Kanai, Y. Examining real-time time-dependent density functional theory nonequilibrium simulations for the calculation of electronic stopping power. *Physical Review B* **2017**, *96*, 115134.

(111) Schleife, A.; Kanai, Y.; Correa, A. A. Accurate atomistic first-principles calculations of electronic stopping. *Physical Review B* **2015**, *91*, 014306.

(112) Quashie, E. E.; Correa, A. A. Electronic stopping power of protons and alpha particles in nickel. *Physical Review B* **2018**, *98*, 235122.

(113) Maliyov, I.; Crocombette, J.-P.; Bruneval, F. Electronic stopping power from time-dependent density-functional theory in Gaussian basis. *The European Physical Journal B* **2018**, *91*, 1–7.

(114) Haque, A.; Mohammadi, A.; Nikjoo, H. Study of the Stopping Power and Straggling for Alpha Particles and Protons in Organic Solids, Liquids and Gases. *13*, 71–74.

(115) Palmer, R. B. J. The stopping power of organic liquids for alpha particles over the energy range 1-8 MeV. *6*, 384.

(116) Araujo, L. L.; Grande, P. L.; Behar, M.; Dias, J. F.; Lifschitz, A. F.; Arista, N. R.; Schiwietz, G. Electronic energy loss of channeled ions: The giant Barkas effect. *70*, 032903, Publisher: American Physical Society.

(117) Andersen, L. H.; Hvelplund, P.; Knudsen, H.; Möller, S. P.; Pedersen, J. O. P.; Uggerhöj, E.; Elsener, K.; Morenzoni, E. Measurement of the ${Z}_{1}^{3}$ contribution to the stopping power using MeV protons and antiprotons: The Barkas effect. *62*, 1731–1734, Publisher: American Physical Society.

(118) Lee, C.-W.; Stewart, J. A.; Dingreville, R.; Foiles, S. M.; Schleife, A. Multiscale simulations of electron and ion dynamics in self-irradiated silicon. *Physical Review B* **2020**, *102*, 024107.